Trans. JWRI, Vol. 24 (1995), No. 2

Prediction Algorithm for Solid State Diffusion Bonding in The Case When Material Constants Are Unknown----Surpport System of Optimum Condition of Solid State Joining Process----†

Yasuo TAKAHASHI*, Koji MIKI, and Katsunori INOUE*****

Abstract

The purpose of the present study is to predict the diffusion bonding process of materials for which the model parameters (material constants) are unknown. Material constants are necessary for the numerical model developed, but the material constants are arranged into seven model parameters, except for the yield stress. We estimate the values of the seven parameters by inverse analysis. We propose the methods to choose the experimental conditions which we need for the inverse analysis. We also propose the algorithm to obtain the proper converged solutions of the unknown model parameters. We indicate that the solutions converge to true model parameters. Further, we show that bonding processes with unknown parameters can be predicted by our algorithm.

KEY WORDS: (Solid state bonding) (Bonding process) (Modelling) (Inverse analysis) (Computer simulation) (Optimum condition)

1. Introduction

The authors have developed a support-system for determining optimum conditions of solid phase bonding by using a numerical model. The numerical model predicts the bonding process for the materials with known material constants[1,2] but it is powerless if the material constants are unknown. The numerical model needs more than twenty material constants, which can be combined down to 8 model parameters, i.e., yield stress of plastic deformation, three parameters of creep deformation, two parameters of interface diffusion and two parameters of volume diffusion by taking into account the void shrinkage process[3,4].

If we can estimate the unknown model parameters then we can predict the bonding processes without the material constant. We need experimental data from several bonding tests. The least experimental data are the most desirable. It is a problem how to minimise the trial number m of the bonding tests.

It is very useful to know the necessary bonding conditions before carrying out the bonding tests. In the present study, we indicate how to choose the necessary bonding conditions, taking into account the bonding mechanisms. And also, we develop the algorithm for estimating unknown model parameters. We further apply the algorithm to the prediction for Ni-Ni bonding process.

2. Forward Analysis for Bonding Prediction

2. 1 Numerical model

We consider the bonding process for similar materials. The previous papers [1, 3, 4] have detailed the numerical model which we summarize here. The numerical model needs the geometrical parameters derived from faying surface profiles; the asperity height h_{oo}, the asperity pitch $2L_{oo}$ and the void spacing $2L$ (see **Fig. 1**). Half the void spacing L changes during bonding[1]. We measured the faying surface profiles by a roughness measuring instrument and fed them into a personal computer through an A to D converter. The change of L is estimated as a function of S by the overlap method [1], in which two faying surface profiles are brought together and gradually overlapped on screen using a graphics package of the computer. The overlap-segments of the two surface profiles are treated as the bonded area X ($=\Sigma_i X_i / n_s$, where n_s is the number of overlap-segments). The distance between unbonded areas gives half the void spacing L. The percentage bonded area S is obtained from X/L. Because $L \cdot n_s$ is always constant, S depends only on X.

We treat the yield stress σ_Y as a known parameter since it can be estimated from the initial contact area X_o at $t = +0$ s, where t is the bonding time, i.e., X_o is given by

† Received on November 24, 1996
* Assosiate Professor
** Graduate Student, Osaka University
*** Professor

Transaction of JWRI is published by Welding Research Institute of Osaka University, Ibaraki, Osaka 567, Japan

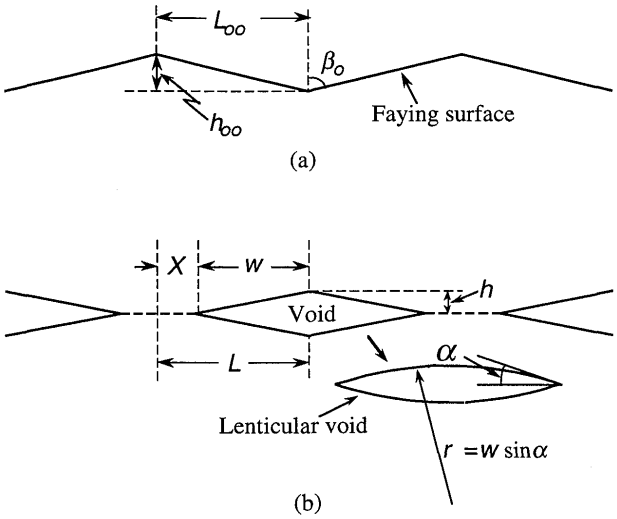

Fig. 1 A two dimensional bonding model, (a) faying surface, (b) bonded interface.

$$X_o = LP/\{(1+\beta_0)\cdot\sigma_Y\}\ , \tag{1}$$

where P is the bonding pressure and β_o is referred to in **Fig. 1**.

We assume that the interfacial contact process is the rate determining step of the bonding process. The interfacial contact is produced by three bonding mechanisms, creep deformation, interface self-diffusion and volume self-diffusion. The voids are approximated to a lenticular shape in considering the diffusion mechanisms and the rate of surface diffusion is high enough to keep the void curvature radius r constant as shown in **Fig. 1** (b). The surface diffusion is then ignored according to ref. [4].

2. 2 Model parameters

According to refs[1, 4], the seven parameters with respect to the material constants are given as follows;

A_c^* (= $A_o \cdot D_{vo} \cdot b \cdot G^{1-n}$), n, and Q_c for the creep deformation, where A_o is a non-dimensional constant, D_{vo} the frequent factor of volume self-diffusion, b Burgers vector, G the shear modulus, n the stress exponent of creep strain rate, and Q_c is the activation energy for creep (A_c^* is a function of G^{1-n} but we assume A_c^* is a constant),

D_{bo}^* (= $D_{bo} \cdot \delta_b \cdot \Omega$) and Q_b for the interface self-diffusion, where D_{bo} is the frequency factor of the interface self-diffusion, δ_b the thickness of the interface, Ω the atomic volume and Q_b is the activation energy for the interface self-diffusion, and also D_{vo}^* (= $D_{vo} \cdot \Omega/\pi$) and Q_v for the volume self-diffusion, where Q_v is the activation energy for the volume self-diffusion and π has the usual meaning.

2. 3 Equations of bonding mechanisms

According to refs[1, 4], the growth rate of X by the creep deformation is given by

$$\dot{X}_c = \frac{A_c^*}{kT}\cdot g(L,X,n)\cdot P^n \exp\left(-\frac{Q_c}{RT}\right)\ , \tag{2}$$

where T is the bonding temperature in Kelvin, k Boltzmann's constant, R the gas constant, and $g(L, X, n)$ is a geometric function of L, X and n. The growth rates of X due to the interface self-diffusion and the volume self-diffusion are, respectively, expressed by

$$\dot{X}_b = \frac{D_{bo}^*}{kT}\cdot g(L,X,r,\alpha) \times\left(\frac{L}{X}P+\frac{\gamma_s}{r}\right)\cdot\exp\left(-\frac{Q_b}{RT}\right) \tag{3}$$

and

$$\dot{X}_v = \frac{D_{vo}^*}{kT}\cdot g(L,X,r,\alpha) \times\left(\frac{L}{X}P+\frac{\gamma_s}{r}\right)\cdot\exp\left(-\frac{Q_v}{RT}\right), \tag{4}$$

where γ_s is the surface tension, $g(L, X, r, \alpha)$ a geometric function, and α is half the dihedral angle at the void tip (see **Fig. 1** (b)).

2. 4 Prediction of bonding process

Figure 2 shows the flow charts of forward problems (a) and the numerical calculation of the bonding process (b). **Figure 3** shows the comparison between experimental percentage bonded area S_e and calculated S_c. The change

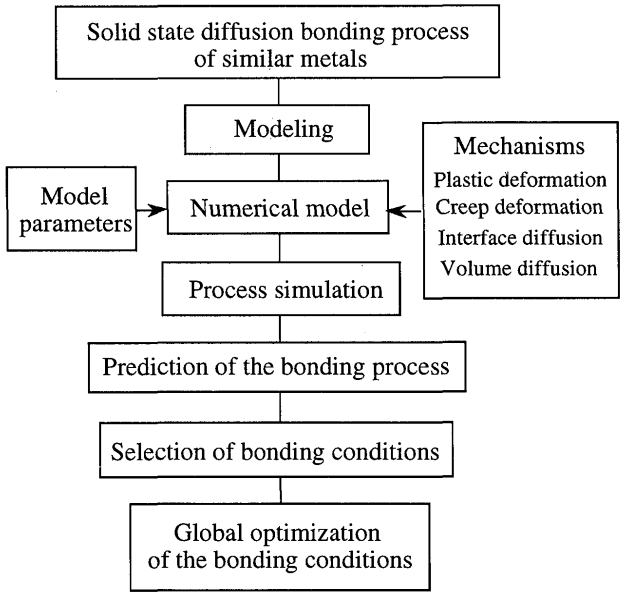

(a)

Fig. 2 The flow charts of forward analysis, (a) for determining the bonding condition.

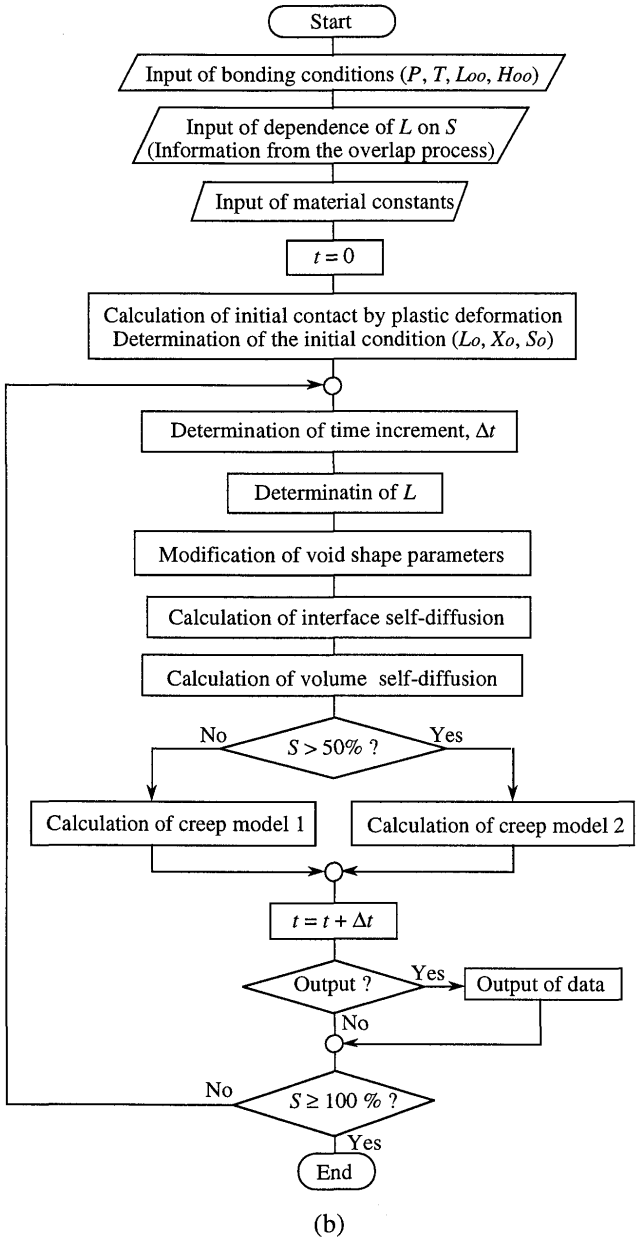

(b)

Fig. 2 Continued.
(b) for predicting the bonding process.

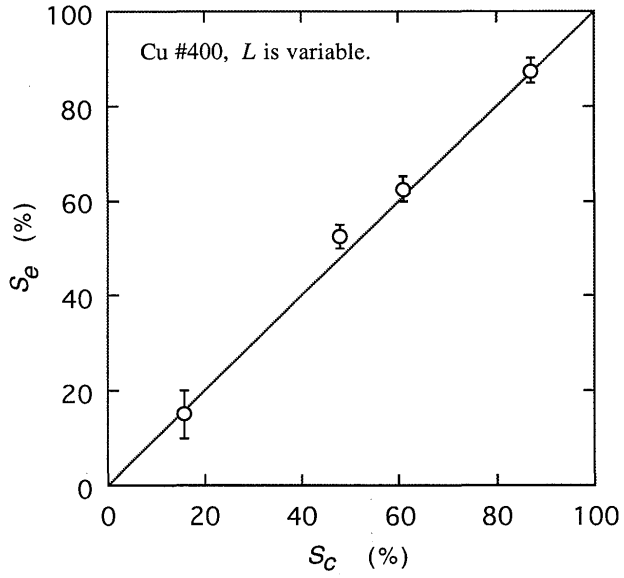

Fig. 3 Verification of the numerical model.

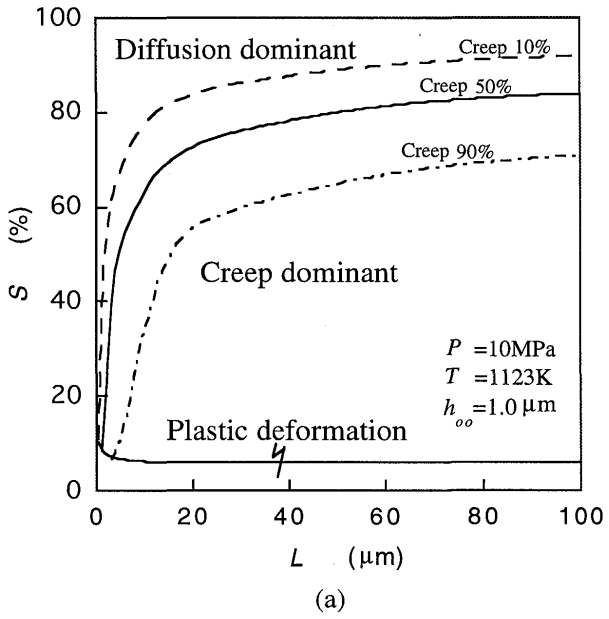

(a)

Fig. 4 Bonding mechanism maps obtained by the numerical model, (a) a *L-S* map.

of L was taken into account in calculating the bonding process. As seen in **Fig. 3**, S_e and S_c agree well, i.e., the numerical model can predict the bonding process if the model parameters are known [1, 2].

Equations (2), (3) and (4) indicate that the three bonding mechanisms depend on L, P, and T. **Figure 4** shows the transition of the dominant mechanisms. The creep deformation becomes dominant as L or P increases. On the other hand, the diffusion mechanism becomes dominant as L and P decrease and contributes significantly even when temperature is low. The contributions of interface and volume self-diffusion change with T and L as shown in **Fig. 5**. *I/D* means the ratio of interface diffusion to total contribution of the diffusion (interface +volume). In other words, the dominant region of each mechanism has a certain tendency, which is summarized in **Table 1**. Normalized pressure P/G and Homologous temperature T/T_m are useful to generalize the dominant region.

3. Inverse Analysis for Bonding Prediction of Materials with Unknown Parameters

Figure 6 shows a flow chart of the inverse analysis to estimate unknown model parameters. This is for estimating 7 parameters at once. We need the numerical model which we used in the forward analysis. The objective function is

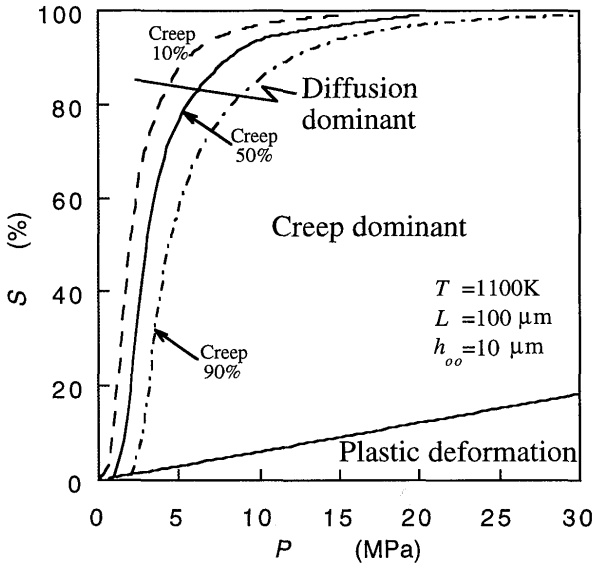

(b)

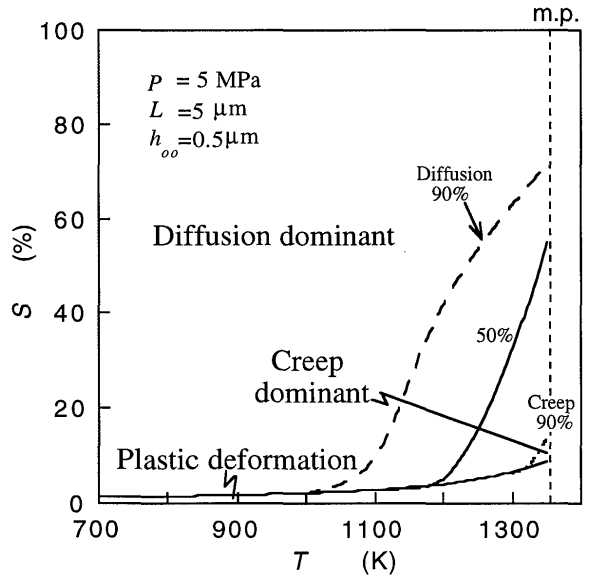

(c)

Fig. 4 Continued.
(b) a *P*-*S* map, and (c) a *T*-*S* map. The mark of m.p. means the melting point..

given by

$$F = \sum_{i=1}^{m} \{(\ln Se_i - \ln Sc_i)/\ln Se_i\}^2, \qquad (5)$$

where Se is the percentage bonded area obtained by the experimental bonding tests and Sc is calculated by the numerical model. We can normalize F if we divide ($\ln Se_i$-$\ln Sc_i$) by $\ln Se_i$ to make the weight equal between $\ln Se_i$.

The variable Se_i should have been experimental but in the present study we use the percentage bonded area calculated by using the material constants of pure copper

Table 1 Dominant mechanism regions.

Bonding mechanisms	Bonding conditions		
	Pressure P	Temperature T	Half void spacing L
Creep deformation	High enough $P/G > 5\times10^{-4}$ ($P > 10$ MPa for Cu)	High $T/Tm > 0.7\sim0.75$ ($T > 1000$ K for Cu)	Large enough $L > 80\mu m$ (coarse surface asperity)
Interface diffusion	Low enough $P/G < 2\times10^{-4}$ ($P < 5$ MPa for Cu)	Low $T/Tm < 0.7\sim0.75$ ($T < 1000$ K for Cu)	Small enough $L < 10\mu m$ (fine surface asperity)
Volume diffusion	Low enough $P/G < 2\times10^{-4}$ ($P < 5$ MPa for Cu)	High $T/Tm < 0.7\sim0.75$ ($T < 1000$ K for Cu)	Large $L > 10\mu m$ (middle surface asperity)

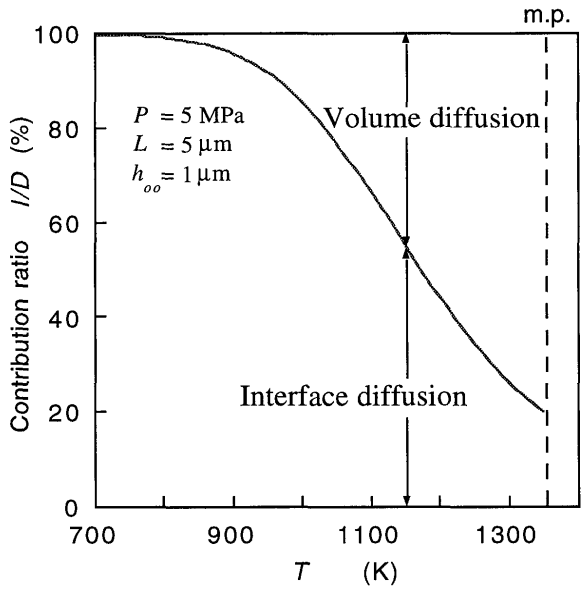

Fig. 5 Contribution of interface self-diffusion to the overall diffusion.

on behalf of experimental S. In that stage, we substituted plausible values as the initial model parameters. We need to choose the proper bonding conditions (P_i, T_i, t_i) and the surface profiles (L_{oo}, h_{oo}) to obtain the experimental data Se_i. We tried to optimize the seven model parameters at once by the steepest descent method but we were not able to obtain any global convergence. The random search required lots of time and it was not possible to find the true model parameter when the bonding conditions (P_i, T_i, t_i, Se_i) ($i = 1$ to m) were not proper. We must adopt another method to find the global convergence. We need also the method for selecting proper bonding conditions. We adopted a two stage search process as stated below. At first, we estimate model parameters for each dominant mechanism and after that we carry out a global search for all model parameters.

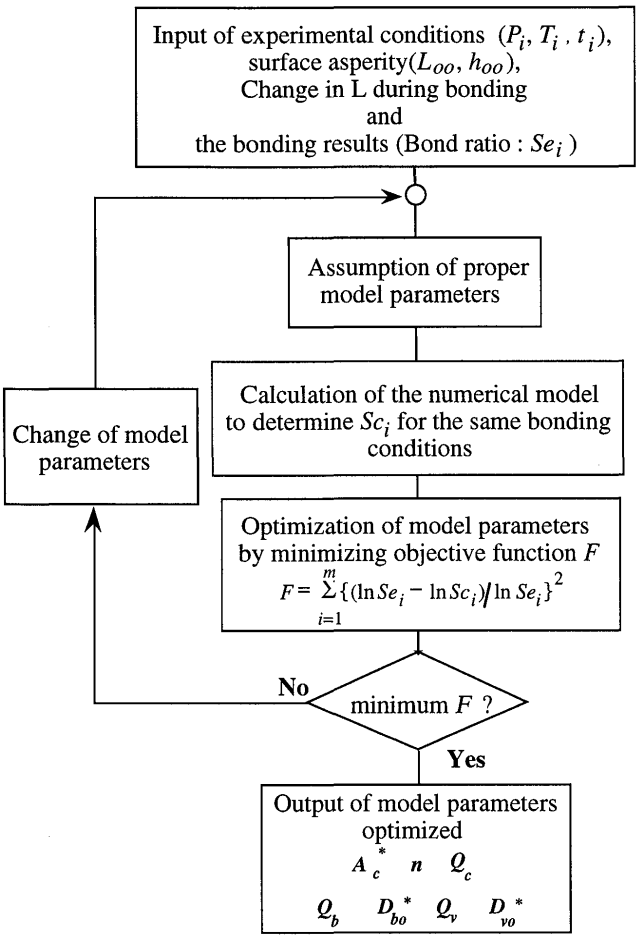

Fig. 6 An algorithm of inverse analysis by estimating seven model parameters at once.

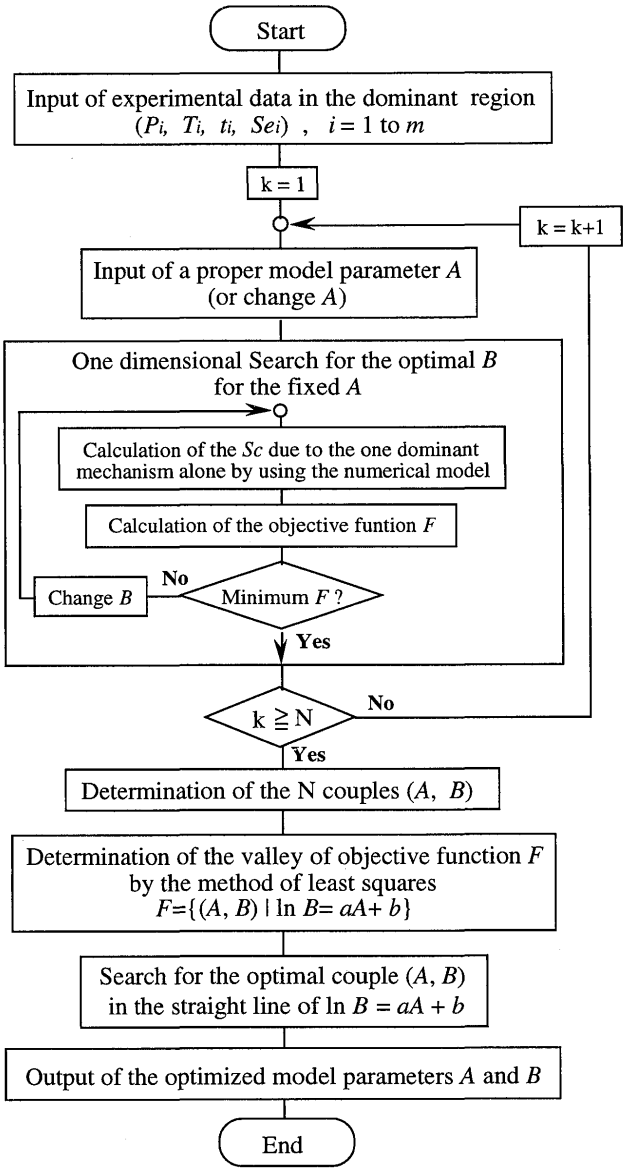

Fig. 7 The algorithm of the preliminary optimization .

4. Estimation of Model Parameters in Dominant Region

We can choose the bonding conditions where creep or diffusion is dominant as shown in **Table 1**. We consider the convergency in the dominant region where one bonding mechanism is dominant. We can decrease the number of parameters from 7 to 2, i.e., we can solve the unknown parameters as a two factor problem.

4. 1 Existence of solution

Let us consider that the bonding is produced by interface diffusion alone. Half the void spacing L changes during bondingbut it is permissible to assume $\dot{S} \approx \dot{X}/L_m$, where L_m is the mean values of L at each S. According to the mean theorem[5], S (or increment ΔS) is represented by

$$S = \frac{D_{bo}^*}{kT} \cdot \exp\left(-\frac{Q_b}{RT}\right) \int_0^t \psi \, dt$$

$$= \frac{D_{bo}^*}{kT} \cdot \exp\left(-\frac{Q_b}{RT}\right) \cdot \bar{g} \cdot t \,, \qquad (6)$$

where $\psi = g(L,X,r,\alpha) \cdot \left(\frac{L}{X}P + \frac{\gamma_s}{r}\right)$, $\bar{g} = \frac{1}{t}\int_0^t \psi \, dt$ and t is the bonding time.

We set the several experimental data (P_i , T_i , t_i , Se_i) obtained in the region where the interface diffusion is dominant (i = 1 to m). After substituting eq.(6) for eq. (5) and arranging eq. (5), we obtain

$$F = \sum_{i=1}^{m} \left\{1 - \lambda_i\left(\ln a_i + \ln D_{bo}^* + b_i Q_b\right)\right\}^2 \,, \qquad (7)$$

where $a_i = \frac{\bar{g}_i \cdot t_i}{kT_i}$, $b_i = -\frac{1}{RT_i}$ and $\lambda_i = \ln Se_i$. Because the second partial derivatives of F with respect to ln D_{bo}* and

Q_b are always greater than zero, the condition of the minimal F is just given by

$$\partial F/\partial Q_b = 0 \quad \text{and} \quad \partial F/\partial \ln D_{bo}{}^{*} = 0. \tag{8}$$

After substituting eq. (7) for eq. (8), we obtain two equations which express two straight lines in the coordinate (Q_b , ln D_{bo}*), i.e.,

$$\ln D_{bo}{}^{*} = \alpha_1 \cdot Q_b + \beta_1 \tag{9}$$

from $\partial F/\partial Q_b = 0$, and

$$\ln D_{bo}{}^{*} = \alpha_2 \cdot Q_b + \beta_2 \tag{10}$$

from $\partial F/\partial \ln D_{bo}{}^{*} = 0$, where α_1, β_1, α_2 and β_2 are given by

$$\alpha_1 = -\frac{\sum_{i=1}^{m}(\lambda_i \cdot b_i)^2}{\sum_{i=1}^{m}\lambda_i{}^2 \cdot b_i}, \tag{11}$$

$$\beta_1 = \frac{\sum_{i=1}^{m}\{\lambda_i b_i(1-\lambda_i \cdot \ln a_i)\}}{\sum_{i=1}^{m}\lambda_i{}^2 \cdot b_i}, \tag{12}$$

$$\alpha_2 = -\frac{\sum_{i=1}^{m}(\lambda_i{}^2 \cdot b_i)}{\sum_{i=1}^{m}\lambda_i{}^2}, \tag{13}$$

and

$$\beta_2 = \frac{\sum_{i=1}^{m}\{\lambda_i(1-\lambda_i \cdot \ln a_i)\}}{\sum_{i=1}^{m}\lambda_i{}^2} \tag{14}$$

respectively. We have to change T_i (i = 1 to m) or α_1 becomes equal to α_2. We can obtain the optimal couple (Q_b , lnD_{bo}) as the intersection of the straight lines (9) and (10).

In the same manner, we can prove the existence of the minimum point of the objective function for the optimal couples (Q_v , lnD_{vo}) and (Q_c, lnA_c*) when the value of n is known. We need the numerical analyses for the geometrical factors $\bar{g}_i$. In fact, we adopted the algorithm as shown in **Fig. 7** where the algorithm of the forward analysis is applied to the inverse analysis without modification.

When the value of n is unknown, we treat a couple (n , lnA_c**), where A_c** is given by

$$A_c{}^{**} = A_c{}^{*} \exp(-Q_c / RT). \tag{15}$$

In that stage, the bonding temperature is fixed. As $g(L, X, n)$ depends on n, $\partial F/\partial n = 0$ does not give a straight line but $\partial F/\partial \ln A_c{}^{**} = 0$ gives a straight line of $\partial F/\partial \ln A_c{}^{**} = 0$. The optimal point (ln$A_c$**, n) exists on it. We can also use the algorithm in **Fig. 7** for estimating the value of n.

Therefore, We conclude that the couples (A, B) in the two factor problem can be an initial basic feasible solution in each dominant region. The algorithm in **Fig. 7** is called the preliminary optimization after this.

4. 2 Convergence to the true values

Figure 8 shows the convergence to the true values with respect to the couples (n, ln A_c**) and (Q_c, lnA_c*). If we choose the bonding conditions where the creep deformation is dominant (P>20MPa, L>80mm, S < 50%)

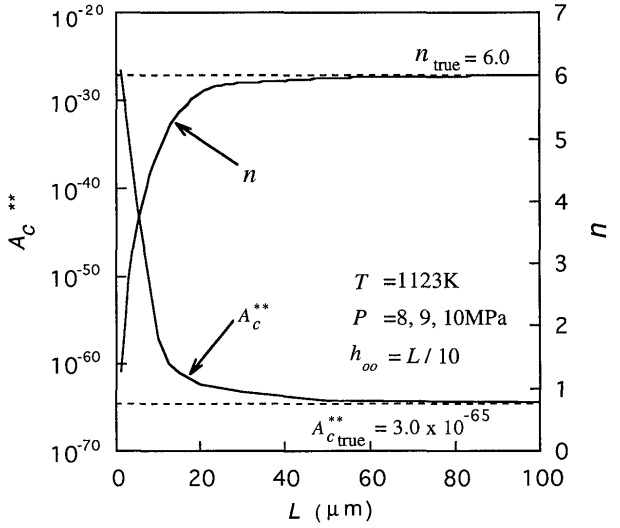

(a)

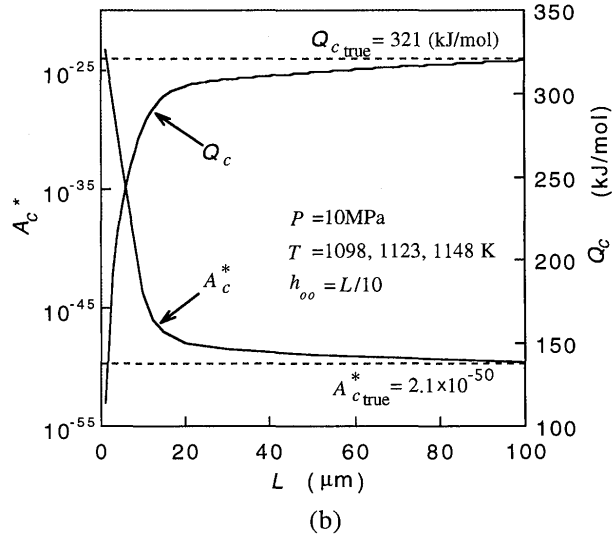

(b)

Fig. 8 Convergence of preliminary optimization for the creep parameters as L increases.
(a) (n , A_c**) solved by changing P, (b) (Q_c , A_c*) solved by changing T.

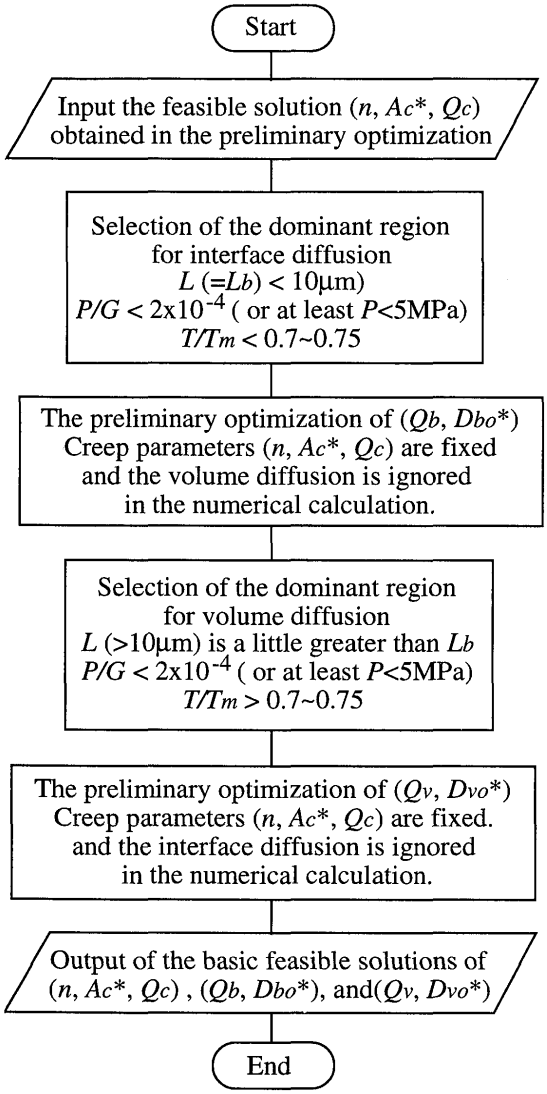

Fig. 9 The algorithm of the overall preliminary optimization.

Table 2 Tendency in deviation of model parameters from true values.

Mechanisms	Deviation of model parameters
Creep deformation	$A_c^* > A_{c\,true}^*$, $n < n_{true}$, $Q_c < Q_{c\,true}$
Interface diffusion	$Q_b > Q_{b_{true}}$, $D_{bo}^* > D_{bo\,true}^*$
Volume diffusion	$Q_v < Q_{v\,true}$, $D_{vo}^* < D_{vo\,true}^*$

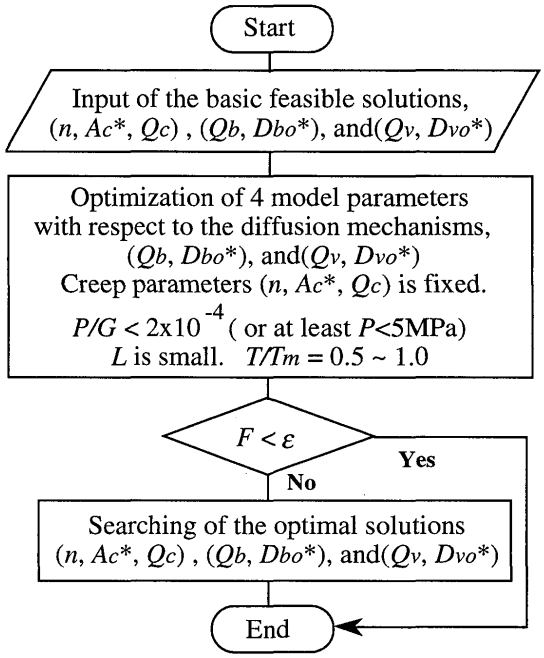

Fig. 10 The algorithm of the final optimization.

then we have the true values.

Figure 9 shows the procedure of the overall preliminary optimization. According to **Table 1**, we chose the three ~ five bonding conditions (m = 3~5) for each preliminary searching. The parameters (n, A_c*, Q_c) easily converge to the true value but it is rather difficult to obtain the true solution (Q_v, D_{vo}*), because the volume diffusion mechanism is not separated perfectly from the interface diffusion. If we obtain a very small F in solving (Q_b, D_{bo}*), we can treat it as a true value. And also we found that all converged solutions tend to deviate from true values as indicated in **Table 2**.

5. Final Optimization

We performed the final optimization as shown in **Fig. 10**. We first used the steepest descent method by fixing the creep parameters. After that, we used a random search method, taking into account the direction of deviation (see **Table 2**). We used all the experimental data adopted in the preliminary optimization (It is better to add the new data obtained in the region where all bonding mechanisms operate). The minimum ε in **Fig. 10** depends on the experimental errors but was less than $6x10^{-2}$ if the errors are kept at within ± 5%.

Table 3 shows the convergence of the final optimization. The converged values are close to the true ones. The number of the data was between 12 and 25. We need at least 7 in total with 2 points in each (we need at least 3 points for creep parameters). This is only theoretical. Actually, we need at least 5~6 points in each preliminary search taking into account the error in experiments. If the error was kept within 5%, we obtained a good convergence. We correctly estimated 7 model parameters from only 25 bonding tests. If we have a smaller error, we can decrease the number of bonding tests to12 points (3 in each).

As mentioned above, our prediction algorithm consists of two optimization steps;

Table 3 Converged values in the final optimization for copper.

Model parameters	Optimized solutions for Cu	True values for Cu
A_c^*	2.48×10^{-50}	2.4×10^{-50}
n	5.99	6.0
Q_c (kJ/mol)	320.0	321
D_{bo}^* (m^6/s)	6.13×10^{-44}	6.0×10^{-44}
Q_b(kJ/mol)	106.0	105
D_{vo}^* (m^5/s)	2.40×10^{-34}	2.3×10^{-34}
Q_v (kJ/mol)	207.0	208
F	4.78×10^{-4} (without errors)	———

(i) The preliminary optimization which should be performed in the dominant region where one bonding mechanism is dominant, and

(ii) the final optimization which starts from the basic feasible solutions of the preliminal optimization.

6. Prediction of Bonding Process of Materials with Unknown Parameters

We had many data for nickel [6, 7] but were not able to find suitable model parameters from the literature except for the yield stress [8]. We, therefore, applied the algorithm developed in the present study to estimate the model parameters for Ni-Ni solid state bonding process.

6. 1 Preparation of faying surfaces and experimental procedure

The material used was a pure nickel the chemical compositions of which is shown in **Table 4**. The nickel specimens were made from cold drawn rod with a 10 mm diameters. The faying surface were machined by a precision lathe to make triangular ridges. The pitch of the ridges L_{oo} was about 100 μm. We also prepared nickel specimens is dominant. The latter were for the region where the diffusion mechanism is dominant.

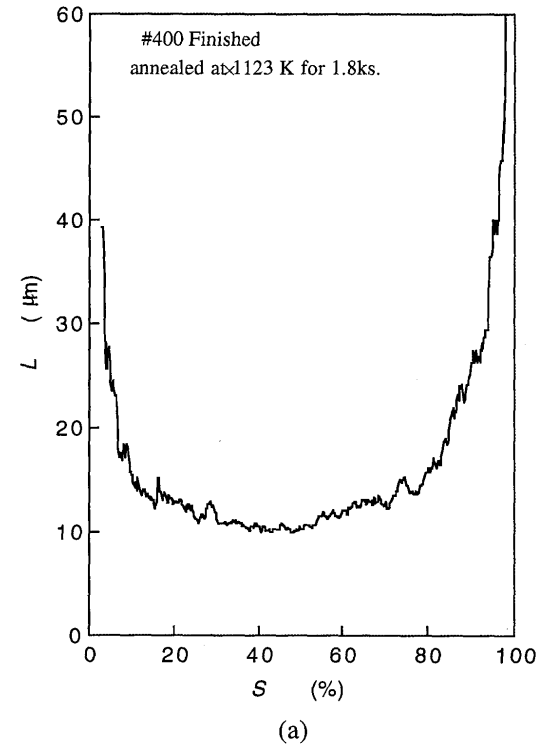

(a)

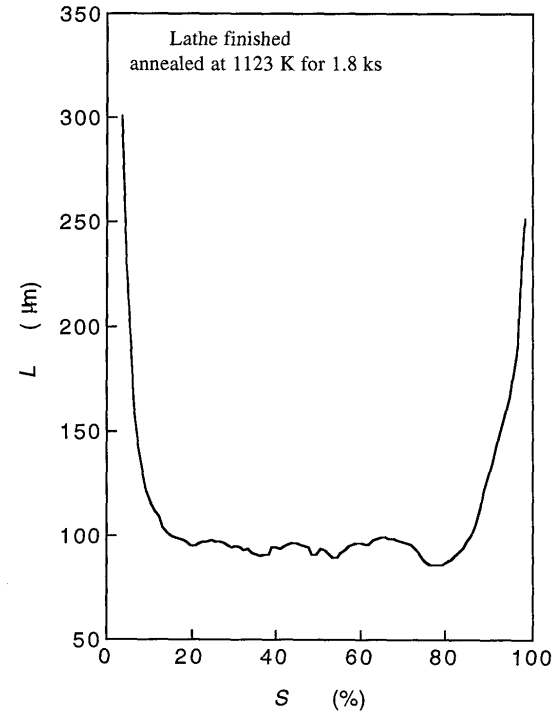

(b)

Fig. 11 *S-L* curves of Ni specimens.
(a) for #400 emery paper,
(b) for lathe finished surface.

Table 4 Chemical compositions (mass%) of a purenickel

Cu	Fe	Si	Mn	C	S	Al	Cr	Ti	Ni
n,d.	0.004	0.003	n,d.	0.004	0.001	n,d.	n,d.	n,d.	Bal.

n.d. : not detected.

Table 5 Bonding conditions for Ni-Ni bonding.

Void spacing L (μm)	Asperity height h_{oo} (μm)	Pressure P (MPa)	Temperature T (K)	Bonding time t (s)	Bond ratio S (%)
					38.9
					37.9
≒100	≒10	20	1273	2619	38.7
					39.7
					39.0
					39.9
					40.0
≒100	≒10	20	1323	941	39.8
					40.5
					61.6
					62.1
5～10	0.5～1.0	5	1173	4799	60.9
					61.2
					61.7
					36.4
					35.5
5～10	0.5～1.0	5	1123	7973	37.1
					36.8
					36.1
					53.1
					51.8
10～15	1.0～1.5	5	1473	2780	52.0
					51.3
					51.3
					52.2
					52.0
10～15	1.0～1.5	5	1423	7776	51.7
					51.5
					50.5

The values of L for S=50% are listed.

Table 6 Converged solution of Ni model parameters compared with general values.

Model parameters	Optimal solutions	General value
A_c^*	2.8×10^{-59}	1.1×10^{-69}～1.1×10^{-47}
n	6.48	4.6～7.5
Q_c (kJ/mol)	323	285～434
Q_b (kJ/mol)	68	115～118
D_{bo}^* (m^6/s)	2.0×10^{-46}	9.6×10^{-45}～3.8×10^{-44}
Q_v (kJ/mol)	320	271～285
D_{vo}^* (m^5/s)	2.0×10^{-32}	2.1～6.6×10^{-34}
F	5.98×10^{-2}	———

Our numerical model needs the S-L relationships as shown in **Fig. 11**. Figure (a) is for #400 emery paper and figure (b) for lathe machining. The S-L relationships were calculated by the overlap method which has been detailed elsewhere [2]. In the present study, the mean values were adopted for L.

Bonding tests were carried out in a vacuum atmosphere ($1.0\text{x}10^{-3}$ Pa). The range of bonding pressures and temperatures were from 5 to 20 MPa and from 1250 K to 1450 K, respectively, that is, the bonding conditions were determined as indicated in **Table 5**. If the bond ratio (percentage bonded area) S was greater than 80 %, the experimental error became large. We adopted the bonding conditions so that S was less than 80 %. The data in **Table 5** were used in the inverse analysis for Ni model parameters.

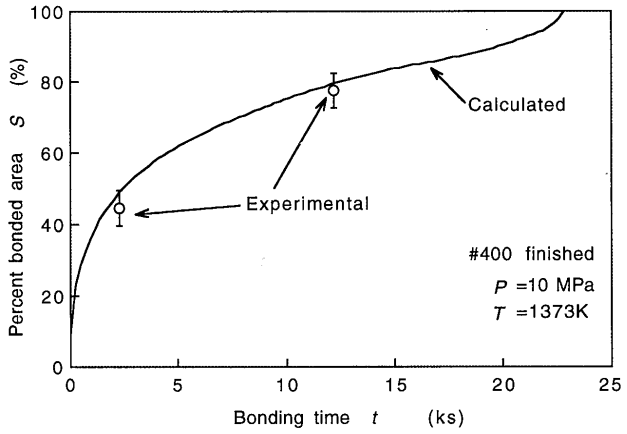

(a)

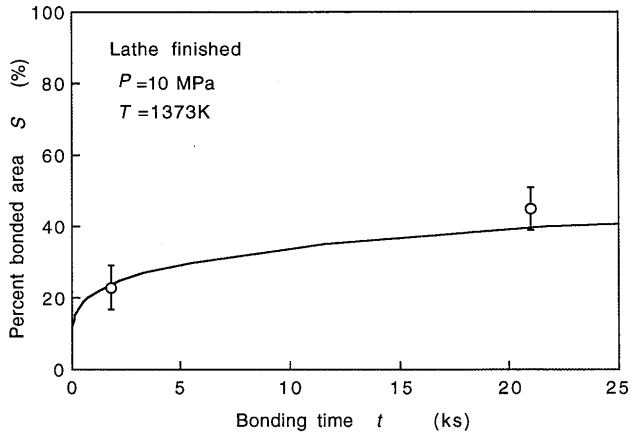

(b)

Fig. 12 Comparision between calculated and experimental results
(a) for the specimen surface finished with #400 emery paper,
(b) for the specimen with lathe machining surface

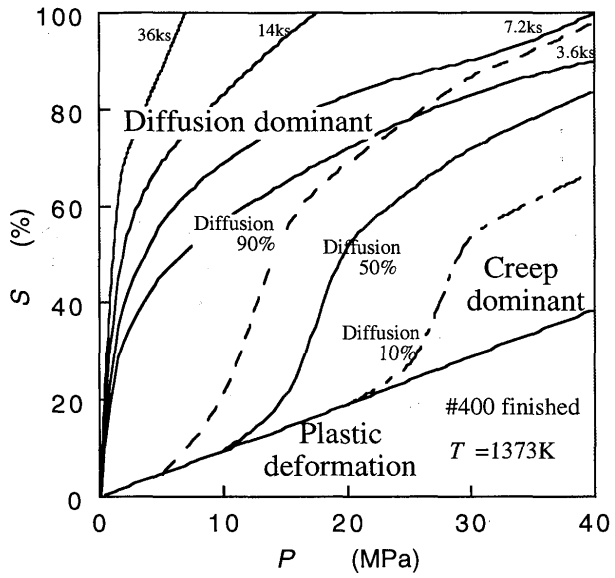

Fig. 13 A Bonding mechanism map of Ni-Ni bonding (*P-S* diagram).

6. 2 Results of Prediction

We optimized the model parameters of nickel according to the prediction algorithm developed in the present study. **Table 6** shows a converged solution of the final optimization. The converged value of the objective function F is larger than 10^{-2}. This is due to the experimental error(10%).

The model parameters estimated were around the general values reported previously[6, 7], except for the activation energy Q_b, which is much less than expected values (100-120 kJ/mol). This may be due to neck growth at bonded areas by surface diffusion which becomes active in the low temperature region[4] but a detailed reason is not known. D_{bo}* is less lower than general values but this is due to a low value of Q_b.

In other words, the converged value of the frequency factor depends on that of the activation energy and they are linked to each other. Q_v is a little greater than the general values but is nearly equal to Q_c. The dislocation creep mechanism is very often controlled by volume self-diffusion. Q_v = 320 kJ/mol is, therefore, a proper value. This higher value gives D_{vo}* a value of 2.0×10^{-23}, greater than the general values. The general values are not necessaryly true values of the nickel specimen used in the present study.

If we use these converged values as the model parameters then we can predict the Ni-Ni bonding under any test conditions other than **Table 5**. **Figure 12** shows the comparision between the calculated and experimental results as an example. They agree well.

Figure 13 shows an example of the bonding mechanism map for Ni-Ni bonding process. This was drawn for the specimen which was surface finished with #400 surface roughness and annealed at 1173 K for 1800 s. We have already reported the purpose of the bonding mechanism map[9].

As stated above, we can predict the bonding process in the range of T = 1270K to the melting point and P = 0 to 40 MPa by our prediction algorithm.

7. Concluding Remarks

We have developed a theory and algorithm to predict the solid state diffusion bonding of materials with unknown model parameters. If we can estimate the model parameters, we can determine the optimum bonding conditions as mentioned elsewhere [1, 2]. We can establish the support-system for determining the optimum bonding conditions of new materials. The authors believe that the algorithm developed in the present study is much more useful than mathematical (experimental) programming methods without taking into account the bonding mechanisms because our method reduce the trial number m. In addition, our prediction algorithm will give useful information to researchers who try to build the prediction theory of joining process.

References

1) Y. Takahashi, and K. Nishiguchi, " Determination of optimum process conditions in solid phase bonding by a numerical model," Welding in the World, Vol. 27, No. 3/4, (1989) pp.100-113.
2) Y. Takahashi and K. Nishiguchi, " Algorithm for determining bonding conditions in solid state diffusion bonding," The 5th international Symposium of JWS, 17-19, April, (1990) pp.145-150.
3) K. Nishiguchi and Y. Takahashi, " A Quantitative analysis of solid state bonding process based on fundamental bonding mechanisms(Part 1), " Quarterly J. of Japan Weld. Soc., Vol. 3, No. 2, (1985) pp. 303-309 (Japanese).
4) Y. Takahashi, and K. Inoue, "Recent void shrinkage models and their applicability to diffusion bonding," Mater. Sci. and Technol., Vol. 8, (1992) pp. 953-964.
5) Y. Takahashi, K. Inoue and Nishiguchi, "Identification of void shrinkage mechanisms," Acta Metall. Mater., Vol. 41, No.11, (1993) pp. 3077-3084.
6) M. F. Ashby, " A first report on deformation-mechanism maps," Act Metall., Vol. 20 (1972) pp. 887-897.
7) T. Chuang et al., " Non-equiliblium models for diffusive cavitation of grain interfaces," Acta Metall. Vol. 27 (1979), pp. 265-284.
8) M. J. Luton and C. M. Sellars, " Dynamic recrystallization in nickel and nickel-iron allys during high temperature deformation," Acta Metall. Vol. 17 (1969) pp. 1033-1043.
9) Y. Takahashi et al., " Analysis of the solid state bonding process by the diagrams of bonding mechanisms," Quarterly J. of Japan Weld. Soc., Vol. 4, No. 2, (1986) pp. 311-316 (Japanese).